Influence of Monomer Structure and Interaction Asymmetries on the Miscibility and Interfacial Properties of Polyolefin Blends

Jacek Dudowicz* and Karl F. Freed

The James Franck Institute and the Department of Chemistry, University of Chicago, Chicago, Illinois 60637

Received August 9, 1996; Revised Manuscript Received October 29, 1996[⊗]

ABSTRACT: The lattice cluster theory (LCT) is used to study the influence of structural and energetic asymmetries on the miscibilities of binary polyolefin blends. The theory describes monomer molecular structures by using a united atom model for the polyolefins, where each CH_n united atom group occupies a single lattice site and where, for simplicity, both species in each blend are taken to have the same number *(M)* of carbons. In order to isolate the contributions from structural asymmetries, the phase diagrams are first computed for a simplified model in which all CH_n united atom groups interact with the same microscopic energy (ϵ), a model for which Flory-Huggins theory would predict complete miscibility. The ratio of the calculated critical temperature (T_c) to the number *(M)* of carbon atoms per chain correlates very well with a blend topological index *(r)* defined in terms of the fractions of tri- and tetrafunctional carbon atoms in the chains. The presence of tetrafunctional carbons is directly responsible for the failure of an older rule of thumb for predicting blend miscibilities on the basis of the disparity in ratios of the numbers of end to interior (or total) carbon atoms per chain of the two blend components. Introducing energetic asymmetries into the LCT united atom model leads to a rich variety of phase behavior (with upper or lower critical temperatures, or even with both lying in an experimentally accessible range). The LCT computations display the same strong sensitivity of phase diagrams to small changes in the microscopic interaction energies as would arise from the Flory−Huggins theory. Computations of coexistence curves are used in conjunction with a recent compressible theory of interfacial properties to examine the influence of monomer structural asymmetries on the interfacial profiles, widths, and tensions in phase-separated polyolefin blends.

I. Introduction

Considerable scientific interest and technological importance is attached to developing a molecular-based theory which describes and explains the factors controlling the mixing of polymers, the compositions of coexisting phases, and the interfacial behavior. Nowhere is this problem more apparent than for polyolefin mixtures, systems which are generally viewed as being so equivalent chemically that the disparities in their thermodynamics are often ascribed solely to different degrees of chain branching. Recent experimental studies of polyolefin blends by Graessley, Lohse, and coworkers[1,2] reveal that a simple solubility parameter theory successfully explains only 70−80% of their data. An understanding of the origin for the deviations from solubility parameter models is important in providing a deeper insight into the factors governing polyolefin miscibilities. For instance, these deviations probably arise from specific molecular details, and a probe of these molecular features immediately raises the question of relating the solubility parameter model of Graessley *et al.*[1,2] to specific molecular characteristics. Thus, it is necessary to develop generalized polymer theories that include the relevant molecular scale information in order to distinguish between the structures of the different polyolefin monomers and their mutual interactions.

The lattice cluster theory[3] (LCT) is one natural vehicle for accomplishing the above goals.[4] The LCT incorporates two major extensions beyond traditional Flory−Huggins[5] (FH) or Sanchez−Lacombe[6] (SL) theories. First is the explicit description of monomer molecular structure by allowing monomers to occupy several lattice sites as dictated by the actual monomer sizes and shapes. For example, Figure 1 depicts the united atom models for different polyolefin monomers in which each lattice site is covered by a single CH_n group, $n = 0$, 1, 2, or 3. While both FH and SL theories ignore packing- and interaction-induced correlations that produce a nonrandom mixing of the polymer chains, the LCT describes the influence of this nonrandom mixing on thermodynamic properties by developing a highly improved, systematic solution to the extended lattice model that is defined[3] by endowing the monomers with molecular structures.

The LCT has already provided a number of conceptual advances[7] in our understanding of polymer blends. Firstly, the theory has explained the previously enigmatic presence of an important entropic component to the Flory interaction parameter χ as arising from differing molecular sizes and shapes of the monomers. Secondly, our computations and comparisons with experiments for polymer blends have emphasized the crucial physical consequences of treating these systems as compressible.[8−10] This work has led to the LCT predictions,[11,12] subsequently verified by Janssen *et al.*[13] and by Hammouda and Bauer,[14] of a substantial pressure dependence to the small angle neutron scattering χ parameter and, consequently, to the phase behavior of polymer blends. The LCT treatments have likewise established[15] the crucial importance of monomer structure on the thermodynamic and the phase properties of polymer blends, a feature continued in the present work on polyolefin miscibilities. Our LCT computations for diblock copolymers have predicted[16] the existence of a re-entrant type microphase separation transition in diblock systems for which the corresponding homopolymer blends exhibit a lower critical solution temperature phase diagram, a bold prediction recently verified experimentally [for the higher temperature phase of poly(styrene)-*block*-poly(butyl methacrylate)] by Russell and co-workers.[17]

[⊗] Abstract published in *Advance ACS Abstracts,* December 15, 1996.

S0024-9297(96)01205-3 CCC: $12.00

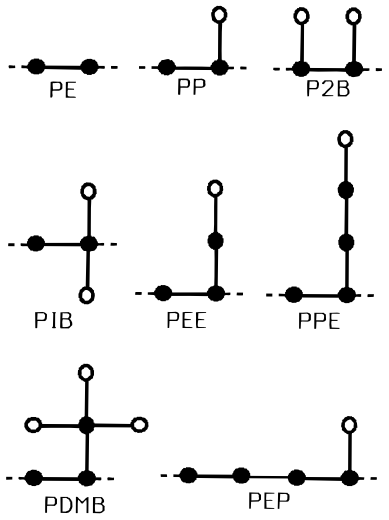

Figure 1. United atom models for monomers of polyethylene (PE), polypropylene (PP), poly(2-butene) (P2B), polyisobutylene (PIB), poly(ethylethylene) (PEE), poly(propylethylene) (PPE), poly(4,4-dimethyl 1-butene) (PDMB), and poly(ethylene−propylene) (PEP). Open circles denote CH_3 end groups, while filled circles designate C, CH, or CH_2 interior groups. Solid lines represent the C−C bonds, and dashed lines indicate groups that are linked to other monomers in the polyolefin chains.

Bates, Frederickson, and co-workers[18] employ a simple incompressible, continuum chain model to stress the importance of disparities in chain flexibilities as having a predominant influence on miscibilities of polyolefins. On the other hand, PRISM computations[19] and the first paper[20] in this series find a considerable role for the enthalpic contributions that are present by virtue of having a compressible system with different propensities for free volume to accumulate about chains with different stiffnesses (in the PRISM computations) or with different monomer structures (in the LCT computations). Work is currently in progress on the inclusion[21] of semiflexibility in the LCT and on its influence on the phase behavior of polymer blends. Preliminary computations for athermal limit semiflexible linear chain systems again display[22] similar general trends as obtained with the PRISM computations. This preliminary work again appears to capture the qualitative features of molecular off-lattice theories, thereby emphasizing the suitability of the LCT for modeling the properties of real systems.

Our focus here on polyolefins arises, in part, from their leading role in the polymer industry. The commercial importance of polyolefins is heightened because the recent development of metallocene catalysts allows the design of polymers with specific desired properties and, thus, the creation of new materials.[23] While the different polyolefins are often considered to be "chemically identical", their miscibilities are observed to differ significantly. For instance, the very immiscible polyethylene/poly(propylene) blend constrasts sharply[24] with the moderate miscibility of poly(propylene) with poly(1-butene). Hence, a small alteration in chemical structures produces profound changes in the blend miscibilities, indicating a strong dependence of miscibility on monomer structure and thereby suggesting the powerful implications of subtle molecular engineering that consists in the strategic placement of methyl, ethyl, etc., groups, with no real change in "chemistry". The goal of the present paper is the development of the theoretical framework for understanding the origins of these miscibility variations. The enormous variability available in polyolefin syntheses makes these systems ideally suited to developing and testing a predictive model for the alteration of phase behavior (and other thermodynamic properties) with small changes in the monomer structure while the overall chemical character of the system is retained.

This paper is a continuation of our previous theoretical studies[20] on the influence of short chain branching on the miscibility of binary polyolefin blends. In particular, we consider more complicated polyolefins with longer branches than the methyl side groups treated in the first paper. One emphasis is placed on developing general guidelines for miscibilities, but another goal lies in predicting systems for which the blends exhibit lower critical solution temperature (LCST) behavior. For example, Graessley, Lohse, and co-workers[2] have indeed found LCST systems with PIB as a component, and their phase behavior remains to be explained from a microscopic standpoint. While our previous work on polyolefin blend miscibilities uses the simplest model of all equal interaction energies in order to focus on the influence of different placements for the methyl side groups, the present LCT calculations also investigate the more realistic energetic asymmetries, which are modeled in binary blends by the presence of (at least) three different interaction energies. The structure- and interaction-induced asymmetries both couple to the "compressibility" (i.e., to nonrandom mixing and to equation of state effects), which further affect the miscibility beyond that predicted by an oversimplistic incompressible model theory. It is worth mentioning that our results contrast sharply with FH theory,[5] which would imply complete miscibility of all the united atom binary polyolefin blends upon use of the simplest model with identical interaction energies. Similarly, SL theory,[6] the generalization of the FH approximation to compressible systems, would likewise predict complete miscibilities of these united atom polyolefin systems when all the SL interaction parameters are taken as equal. The LCT yields nontrivial phase diagrams with this equal energy model because of a coupling between nonrandom mixing and "compressibility" effects.

Section II describes the united atom lattice model of binary polyolefin blends, briefly reviews the basic features of the lattice cluster theory, specifies the constant pressure stability conditions, and outlines the theory[25] of the interfacial properties. Those readers more interested in the results may skip directly to section III, which summarizes the LCT computations of the phase diagrams and discusses various miscibility patterns that arise from the presence of energetic and structural asymmetries between the two blend components. The treatment begins with more extensive model computations focusing on the structural asymmetries. The structural asymmetry is characterized by a topological index *(r)*, and a strong correlation is found between the critical temperature and the index *r*. Interaction asymmetry is then shown to affect the miscibility so strongly that the prediction of precise miscibility patterns is difficult, if not impossible, without the input of empirical information. This strong sensitivity of the phase diagrams to subtle differences in the microscopic interaction mirrors a similar sensitivity within FH theory. The sensitivity stems in FH theory from the fact that the exchange energy,

$$\epsilon_{ex} = \epsilon_{11} + \epsilon_{22} - 2\epsilon_{12} \qquad (1.1)$$

is generally a very small number ($10^{-3} - 10^{-4} k_B T$) even though each of the three interaction energies ($\epsilon_{\alpha\beta}$) is on the order of $k_B T$. A very slight change, for instance, in ϵ_{12} (when ϵ_{11} and ϵ_{22} are fixed) may lead to either positive or negative ϵ_{ex} and, consequently, to completely different types of phase diagrams. Section IV illustrates typical variations of the interfacial profiles, widths, and tensions with monomer structures and, hence, with blend miscibilities.

II. Lattice Cluster Theory of a Binary Blend

A. Model of a Binary Polyolefin Blend. The extended lattice model of a binary blend represents each component α (α = 1 and 2) as n_α monodisperse polymer chains placed on a regular array of N_l lattice sites and coordination number z. A single chain of species α occupies $M_\alpha = N_\alpha s_\alpha$ lattice sites, where N_α is the polymerization index and s_α designates the number of lattice sites covered by a single monomer of species α. The monomer occupancy index s_α may, in general, take any value necessary for realistically describing the monomer size and shape. The monomer structure for a given polyolefin species is chosen as that corresponding to a united atom model in which individual CH_n (n = 0, 1, 2, or 3) united atom groups reside at single lattice sites. Consequently, the occupancy index s_α coincides with the number of the carbon atoms in a single monomer. The bonds between united atom groups represent the $C-C$ bonds. Figure 1 depicts the monomers of several polyolefin species considered in the present LCT computations. Some of the examples exhibited by Figure 1 have already been used in our earlier work,[20] which neglects differences in interaction energies between the different united atom groups in order to focus explictly on probing the influence of short chain branching on blend miscibilities.

The nonzero compressibility of polymer blends implies the existence of excess free volume which is modeled by the presence of n_v empty sites (voids) with volume fraction $\phi_v = n_v/N_l$. The void volume fraction ϕ_v is determined from the equation of state for a given pressure, temperature, unit cell volume, and blend composition. The latter is expressed in terms of the nominal volume fractions $\Phi_1 = 1 - \Phi_2 = n_1 M_1/(n_1 M_1 + n_2 M_2)$ which are simply related to the actual volume fractions $\phi_\alpha \equiv n_\alpha M_\alpha / N_l$ by $\Phi_\alpha = \phi_\alpha/(1 - \phi_v)$. The lattice is taken to be a three-dimensional ($d = 3$) cubic lattice with $z = 2d = 6$.

The interactions between monomers of the same or different species involve short range repulsions and longer range attractions. The former are represented in the lattice model by excluded volume constraints that prohibit the multiple occupancy of any lattice site, while the latter are introduced by ascribing the attractive microscopic van der Waals energy $\epsilon_{\alpha\beta}^{ij}$ to nearest neighbor (on the lattice) portions i and j of monomers α and β. All the s_α united atom portions of a monomer α are taken as energetically equivalent units (i.e., monomer averaged), which interact with any of the s_β portions of a monomer β with the same energy $\epsilon_{\alpha\beta}$. In contrast to our previous use of the simplest equal interaction $\epsilon_{\alpha\beta} \equiv \epsilon$ model for studying the influence of short side group branches on blend miscibility,[20] the three independent monomer averaged interaction energies ϵ_{11}, ϵ_{22}, and ϵ_{12} are allowed here to differ. Thus, they more realistically reflect the large deviations with n, for example, in the Lennard−Jones $(CH_n)-(CH_n)$ interaction parameters used in continuous space simulations[26] of polyolefin melts.

B. Free Energy of a Binary Blend. The lattice cluster theory[3] (LCT) provides the Helmholtz free energy F of a compressible binary blend in the simple analytic form,

$$\frac{F}{N_l k_B T} = \phi_v \ln \phi_v + \sum_{i=1}^{i=2} \frac{\phi_i}{M_i} \ln \frac{2\phi_i}{M_i} - (\ln z - 1) \sum_{i=1}^{i=2} \left(1 - \frac{1}{M_i}\right) \phi_i + \sum_{k=1}^{k^*} \sum_{l=0}^{k} f_{kl} \phi_1^{\,l} \phi_2^{\,k-l} \quad (2.1)$$

The first three terms on the right hand side of eq 2.1 describe the combinatorial part of F, while the last term represents the noncombinatorial portion of F as a polynomial in the actual volume fractions ϕ_1 and ϕ_2. The coefficients f_{kl} in eq 2.1 are generated[3] as double expansions in the inverse lattice coordination number $1/z$ and in the three dimensionless microscopic van der Waals attractive energies $\epsilon_{\alpha\beta}/k_B T$. The coefficients in these double expansions depend on the monomer molecular structures and molecular weights of the two blend components. The present calculations of F are performed through orders $1/z^2$ and $(\epsilon_{\alpha\beta}/k_B T)^2$, which fix[3] the upper limit of k in the double summation in (2.1) as $k^* = 6$. The polynomial form of the f_{kl} in eq 2.1 permits the very rapid computation of constant pressure phase diagrams with a simple PC computer. The computational time is comparable to the time necessary for generating constant pressure binodals (or spinodals) from the Sanchez−Lacomb type[6] free energy expression which is the limit of eq 2.1 with $k \le 2$ and with the f_{kl} treated as constants divided by T.

Polymer blends at constant pressure P are more appropriately described by the Gibbs free energy *(G)*,

$$G = F + PV = F + P N_l v_{cell} \quad (2.2)$$

where the pressure P is computed from eq 2.1 as

$$P \equiv -\left.\frac{\partial F}{\partial V}\right|_{T,n_1,n_2} = -\frac{1}{v_{cell}} \left.\frac{\partial F}{\partial n_v}\right|_{T,n_1,n_2} \quad (2.3)$$

under the assumption that the volume (v_{cell}) associated with one lattice site is a constant. Equations 2.3 and 2.1 produce the equation of state $P = P(\Phi_1, \phi_v, T, v_{cell})$, which enables determining ϕ_v as a function of Φ_1, T, and v_{cell} for a given P. Both the free energies G and F as well as the void volume fraction ϕ_v are quite insensitive to the choice of v_{cell} over wide ranges of pressures and temperatures. Hence, the different polyolefins are assumed, for simplicity, to have the same cell volumes (v_{cell}), but different v_{cell} values may readily be employed in conjunction with standard combining rules.[27]

C. Spinodal Curves and Coexistence Curves at Constant Pressure. Generally, a binary system at constant pressure P and temperature T is stable (or metastable)[28] if

$$\left.\frac{\partial^2 G}{\partial x_1^{\,2}}\right|_{P,T,x_2} > 0 \quad (2.4)$$

where G designates the Gibbs free energy of the whole system and x_i denotes the number of moles of species i. The constraint (2.4) can be conveniently rewritten in terms of the blend composition $\Phi_1 = n_1 M_1/(n_1 M_1 + n_2 M_2)$ as

$$\left.\frac{\partial \mu_1}{\partial \Phi_1}\right|_{P,T} > 0 \tag{2.5}$$

where

$$\mu_1 = \left.\frac{\partial \mathrm{F}}{\partial n_1}\right|_{V,T,n_2} = \left.\frac{\partial G}{\partial n_1}\right|_{P,T,n_2} \tag{2.5a}$$

is chemical potential of polymer species 1. Equating the left hand side of the inequality (2.5) to zero produces the stability limit (called the "spinodal") for the constant pressure binary polymer blend as

$$\left.\frac{\partial \mu_1}{\partial \Phi_1}\right|_{P,T} = 0 \quad \text{(spinodal)} \tag{2.6}$$

The constant pressure derivative $\partial\mu_1/\partial\Phi_1$ is calculated from the LCT free energy expression (2.1) along the lines described previously,[29] and the stability limit is easily converted into the standard form of the spinodal temperature $T_s = T(\Phi_1)$ as a function of composition.

As mentioned above, a binary polymer blend can form a homogeneous phase or a two-phase system. When phase separation occurs at constant pressure P, the coexisting phases (denoted as I and II) have equal pressures and equal chemical potentials for both blend components,

$$\mu_\alpha^{(\mathrm{I})} = \mu_\alpha^{(\mathrm{II})} \qquad \alpha = 1, 2$$

$$P^{(\mathrm{I})} = P \qquad P^{(\mathrm{II})} = P \tag{2.7}$$

The coexistence curve for the binary blend is determined by the set of points $\{T,\Phi_1^{(\mathrm{I})},\Phi_1^{(\mathrm{II})}\}$ satisfying eq 2.7. The coexistence curve and the spinodal curve coincide at the critical point.

D. Interfacial Properties of Phase-Separated Binary Blends. Coexistence curves provide one essential input into theories describing the interfaces between different phases in polymer blends. Since monomer molecular structure strongly affects the phase behavior, it is natural to probe the variation of interfacial properties with monomer structural asymmetries. The theory[25] of interfacial properties of phase-separated compressible binary blends is specialized to planar interfaces (perpendicular to the z axis and centered at $z = 0$). Given two coexisting phases at constant temperature and pressure, the compositions $\phi_1 = \phi_1(z)$ and $\phi_2 = \phi_2(z)$ of both components vary through the planar interface. The total free energy functional **F** of an interface is expressed as the sum of homogeneous and inhomogeneous contributions,

$$\mathbf{F} = \mathbf{F}_\mathrm{h} + \mathbf{F}_\mathrm{inh} \tag{2.8}$$

The inhomogeneous $\mathbf{F}_\mathrm{inh}$ portion of the functional **F** is given by

$$\mathbf{F}_\mathrm{inh} = \frac{1}{k}\int_{-\infty}^{\infty} \mathrm{d}z \left[\frac{{l_1}^2}{s_1\phi_1}\left(\frac{\mathrm{d}\phi_1}{\mathrm{d}z}\right)^2 + \frac{{l_2}^2}{s_2\phi_2}\left(\frac{\mathrm{d}\phi_2}{\mathrm{d}z}\right)^2\right] \tag{2.9}$$

where l_α and s_α are, respectively, the Kuhn length and monomer occupancy index for species α, and where $k = 36$ applies in the weak segregation limit for which the radius of gyration (R_G) is much less than the interfacial width (ω) and $k = 24$ applies in the opposite strong segregation limit. Equation 2.9 has been derived by Tang and Freed[30] for compressible blends in a weak segregation limit as a generalization of the standard random phase approximation (RPA) formula for incompressible systems. Because the coexisting phases are at constant pressure, the homogeneous portion $\mathbf{F}_\mathrm{h}$ of the functional **F** is written as

$$\mathbf{F}_\mathrm{h} = \int_{-\infty}^{\infty} \mathrm{d}z\, [f(\phi_1,\phi_2) - \mu_1^*\phi_1 - \mu_2^*\phi_2 + P v_\mathrm{cell}/k_\mathrm{B}T] \tag{2.10}$$

where $f(\phi_1,\phi_2) \equiv F/(N_1 k_\mathrm{B}T)$ is the specific Helmholtz free energy, P is the constant pressure in the bulk phases, and $\mu_\alpha^* \equiv \mu_\alpha/(M_\alpha k_\mathrm{B}T)$ is the dimensionless chemical potential of polymer species α (in the coexisting phases) per occupied lattice site. The free energy F and chemical potential μ_α are provided by the LCT from eqs 2.1 and 2.5a, respectively. The integrand in eq 2.10 vanishes identically in both homogeneous phases.

Minimizing the free energy functional in eq 2.8 with respect to the independent variations $\delta\phi_1(z)$ and $\delta\phi_2(z)$ leads to the set of two nonlinear second-order differential equations

$$\frac{c_1}{\phi_1}\frac{\mathrm{d}^2\phi_1}{\mathrm{d}z^2} + \frac{c_1}{2{\phi_1}^2}\left(\frac{\mathrm{d}\phi_1}{\mathrm{d}z}\right)^2 + \frac{\partial f}{\partial \phi_1} - \mu_1^* = 0 \tag{2.11a}$$

$$\frac{c_2}{\phi_2}\frac{\mathrm{d}^2\phi_2}{\mathrm{d}z^2} + \frac{c_2}{2{\phi_2}^2}\left(\frac{\mathrm{d}\phi_2}{\mathrm{d}z}\right)^2 + \frac{\partial f}{\partial \phi_2} - \mu_2^* = 0 \tag{2.11b}$$

with the boundary conditions

$$\phi_1(z{=}\infty) = \phi_1^{(\mathrm{I})} \qquad \phi_1(z{=}-\infty) = \phi_1^{(\mathrm{II})} \tag{2.12a}$$

$$\phi_2(z{=}\infty) = \phi_2^{(\mathrm{I})} \qquad \phi_2(z{=}-\infty) = \phi_2^{(\mathrm{II})} \tag{2.12b}$$

where the subscripts I and II refer to the coexisting homogeneous phases and $c_\alpha \equiv 2{l_\alpha}^2/(s_\alpha k)$ with $k = 36$ or 24. The set of second-order nonlinear differential equations in (2.11) is numerically unstable. Therefore, special procedures have been developed[25] based on a combination of variational and perturbation methods to generate the solutions $\phi_1(z)$ and $\phi_2(z)$.

The interfacial width (ω) of the total density profile [$\phi(z)$] is defined through the standard approximation[25]

$$\omega = \left|\frac{\phi^{(\mathrm{I})} - \phi^{(\mathrm{II})}}{\left.\dfrac{\mathrm{d}\phi}{\mathrm{d}z}\right|_{z=0}}\right| \tag{2.13}$$

where $\phi^{(\mathrm{I})} \equiv \phi_1^{(\mathrm{I})} + \phi_2^{(\mathrm{I})}$ and $\phi^{(\mathrm{II})} = \phi_1^{(\mathrm{II})} + \phi_2^{(\mathrm{II})}$ are the sums of the actual volume fractions ϕ_1 and ϕ_2 in the coexisting phass I and II. The interfacial tension (γ) is determined[25] directly by numerical integration,

$$\gamma = -2k_\mathrm{B}T\int_{-\infty}^{\infty} \mathrm{d}z\, \{g[\phi_1(\pm\infty),\phi_2(\pm\infty)] - g[\phi_1(z),\phi_2(z)]\} \tag{2.14}$$

where the quantitity $g[\phi_1(z),\phi_2(z)] \equiv f(\phi_1,\phi_2) - \mu_1^*\phi_1 - \mu_2^*\phi_2$ is the same linear combination of the specific Helmoltz free energy f and the chemical potentials μ_1^* and μ_2^* that appears in eq 2.10.

III. LCT Computations of Phase Diagrams

Our earlier computations[20] of polyolefin blend miscibilities focus on the role of the short chain branching

Table 1. Branching Parameters r_i, p_i, and q_i for the Polyolefin Species with the Structured Monomers Depicted in Figure 1[a]

polyolefin	r_i	p_i	q_i
PE	1	0	0
PEP	1.2	0.2	0.25
PPE	1.2	0.2	0.25
PEE	1.25	0.25	0.33
PP	1.33	0.33	0.5
P2B	1.5	0.5	1
PDMB	1.67	0.5	1
PIB	1.75	0.5	1

[a] All branching parameters are evaluated in the long chain limit.

by employing a model with a single interaction for all united atom groups in the system. A typical polyolefin blend with three identical van der Waals interaction energies $\epsilon_{11} = \epsilon_{22} = \epsilon_{12}$ exhibits only an upper critical solution temperature (UCST) phase diagram. Subsection A begins by extending our previous analysis[20] to polyolefins with branches of various lengths. Subsection B develops a correlation between computed critical temperatures and a previously introduced measure of blend structural asymmetry, which is represented here in terms of more obvious quantities than the combinatorial indices $N_2^{(1)}$ and $N_2^{(2)}$ (defined below) used in our previous work.[20] Subsection C describes the implications of lifting the assumption of a single interaction energy. The inclusion of a more realistic model with energetic asymmetries is shown to affect the computed miscibilities and even the type of phase diagram.

A. Further Studies of Structural Asymmetries. It is obvious that the actual patterns of polymer blend miscibilities must arise from the combined influences of structural and energetic asymmetries between the two blend components. As shown in section II, both of these asymmetries can be explicitly described by the LCT which is specially designed for this purpose. (A recent improvement[22] of the LCT also enables introducing the bending energies characterizing local chain stiffness. Future work with this enhanced LCT model will enable direct comparison with PRISM theory treatments of polyolefin miscibilities and with the assumptions of the Bates−Fredrickson model.)

Much simpler approaches attempt to approximate polyolefin miscibilities based solely on the monomer structures of the two polyolefin species. A general rule of thumb relates miscibilities to differences in the ratio p_i of end to total (or interior) groups in a single chain. Polyolefins with similar values of p_i are believed to mix well, while those with more disparate ratios p_i are supposed to be less miscible. This simple and commonly used measure of polyolefin blend miscibility is predicted by the single interaction energy LCT to fail for polyolefin blends formed from components with the same values of p_i. For instance, PIB, P2B, and PDMB all have the identical $p_i = {}^1/_2$ (see Table 1), but their computed miscibility patterns are quite different. Figure 2 depicts the spinodal curves for the three polyolefin blends PP/PIB, PP/P2B, and PP/PDMB which are characterized by having identical values for $p = |p_{PP} - p_i| = |{}^1/_3 - {}^1/_2| = {}^1/_6$. Both polyolefin species in each blend are taken to have the same numbers $[M_i\ (i = 1,2)]$ of carbon atoms per chain, but the M_i are varied between these three blends in order to prevent the calculated critical temperatures for the less miscible systems (i.e., PP/PIB and PP/PDMB) from exceeding decomposition temperatures. The disparities in the miscibilities of these three binary systems, therefore, greatly exceed initial impressions

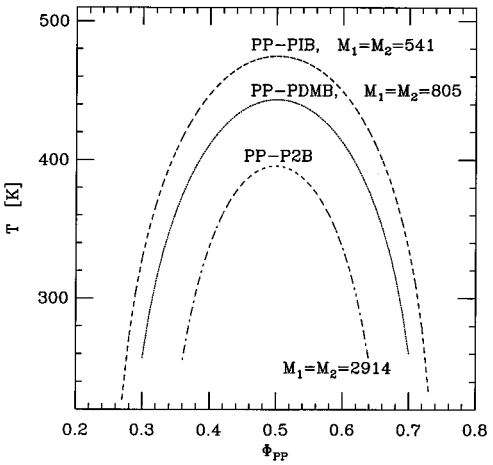

Figure 2. LCT spinodal curves for a series of polyolefin blends (at $P = 1$ atm) with PP as the common component 1. The second component of these three blends has the same ratio p_2 (or q_2) of end to total (or to interior) groups. The phase diagrams are generated for the simple model with three identical interaction energies $\epsilon = \epsilon_{11} = \epsilon_{22} = \epsilon_{12} = 207.75$ K, and the molecular weights are indicated in the figure as the numbers of carbon atoms $M_1 = M_2 = M$ for each blend. The unit cell volume v_{cell} is taken as $(2.5477)^3$ A^3 in Figures 2−16.

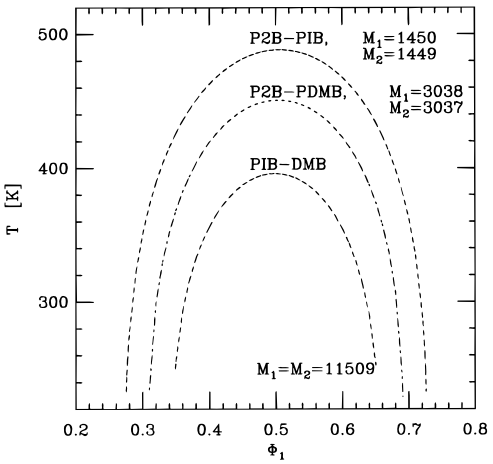

Figure 3. LCT spinodal curves for three polyolefin blends (at $P = 1$ atm) having identical values for the rule of thumb parameter $p = |p_1 - p_2| = 0$ and identical microscopic interaction energies $\epsilon_{11} = \epsilon_{22} = \epsilon_{12} = \epsilon = 207.75$ K.

from the cursory visual comparison of their phase diagrams in Figure 2. The molecular weights for the most miscible PP/P2B blend are a factor of 5 higher than for the least miscible PP/PIB blend ($M_{P2B} = M_{PP} = 2914$ versus $M_{PIB} = M_{PP} = 541$), so computed critical temperatures would exceed a factor of 5 difference when using the same molecular weights for both blends. Thus, for example, complete miscibility emerges for the PP/P2B and PP/PDMB systems from the analogous LCT calculations produced by employing the same low molecular weights ($M_1 = M_2 = 541$) for the all three systems.

Further examples delineating the failure of this rule of thumb are provided in Figure 3, which presents spinodals for three possible binary blends formed from PIB, P2B, and PDMB. As mentioned above, each of these individual polyolefin species yields $p_i = {}^1/_2$. Hence, the rule of thumb would imply that each of the three blends is very miscible since $p = |{}^1/_2 - {}^1/_2| = 0$ is a minimum. In contrast, Figure 3 demonstrates that the miscibilities of these blends are drastically different. Only the P2B/PDMB blend can be considered as a

compatible mixture in the range of moderately large molecular weights.

B. A Predictor of Blend Miscibility Patterns. The first paper in this series introduced a rough correlation between the computed polyolefin miscibilities and several blend properties, such as the small angle neutron scattering effective interaction parameter (χ_{eff}), the volume changes on mixing, and a monomer structural parameter *(r)*. The latter qualitative correlation is extended and quantified here on the basis of many more examples. Before describing this correlation, we briefly note the motivation for its consideration as follows: The LCT free energy of eq 2.1 depends on a whole host of geometrical parameters characterizing the size, shape, and bond connectivity of the united atom groups within the monomers and the polymer chains. The presence of an entropic contribution to χ_{eff} arises from the structural asymmetries between the monomers and is represented likewise in terms of these geometrical parameters. This representation, however, is greatly simplified in the high molecular weight, high pressure limit, whereupon the entropic portion of χ_{eff} becomes proportional[15] to a single combination r^2 of geometrical parameters as described below. Thus, the parameter r^2 provides a natural first choice for investigating a possible correlation with the variations in phase behavior due to monomer structural asymmetries.

The examples in Figures 2 and 3 emphasize the need for a better measure of how blend structural asymmetry affects miscibility. A detailed analysis of the spinodal curves for all the possible binary polyolefin blends, the monomer structures of which are given in Figure 1, indicates the existence of a strong correlation between the blend miscibility and the blend parameter r defined as

$$r = |r_1 - r_2| = \left| \frac{M_1 + M_1^{(tri)} + 3M_1^{(tetr)}}{M_1} - \frac{M_2 + M_2^{(tri)} + 3M_2^{(tetr)}}{M_2} \right| \quad (3.1)$$

where $M_i^{(tri)}$, $M_i^{(tetr)}$, and M_i are the numbers of trifunctional, tetrafunctional, and total carbon atoms, respectively, in a single polyolefin chain of polymer species i. Since carbon cannot be higher than tetrafunctional, the representation (3.1) is exactly equivalent to the more general formula (3.2) of the first paper[20] of this series. Equation 3.1 is, however, much simpler and convenient to apply. The previously used monomer structure dependent coefficient $N_2^{(i)}$ counts the number of distinct sequentially bonded sets of two bonds in a single chain. Equation 3.1 expresses this $N_2^{(i)}$ for a polyolefin chain in terms of the more apparent M_i, $M_i^{(tri)}$, and $M_i^{(tetr)}$ quantities, which can be readily obtained from just trivial counting of the number of different types of united atom groups in the monomer structures of Figure 1. As described in the first paper, the blend miscibility is found to diminish as r increases, and there is a perfect correlation (for fixed M_i) between the magnitudes of r and T_c.

Noticing that the number $M_i^{(e)}$ of end groups in a chain is strictly related[31] to the numbers of tri- and tetrafunctional carbon atoms through

$$M_i^{(e)} = M_i^{(tri)} + 2M_i^{(tetr)} \quad (3.2)$$

Table 2. Correlation of Blend Miscibility with the Blend Branching Parameter *r* for the Model Binary Polyolefin Blends (of Figure 6) at *P* = 1 atm[a]

blend	M_1	M_2	T_c/M (K)	r	p	q
PE/PIB	172	173	2.820	0.75	0.5	1
PE/PDMB	216	217	2.240	0.6667	0.5	1
PPE/PIB	311	313	1.532	0.55	0.3	0.75
PEP/PIB	311	313	1.523	0.55	0.3	0.75
PIB/PEE	353	353	1.238	0.5	0.25	0.6667
PE/P2B	354	354	1.220	0.5	0.5	1
PPE/PDMB	401	403	1.067	0.4667	0.3	0.75
PEP/PDMB	401	403	1.058	0.4667	0.3	0.75
PEE/PDMB	485	487	0.827	0.4167	0.25	0.6667
PP/PIB	484	485	0.815	0.4167	0.1667	0.5
PE/PP	742	742	0.517	0.3333	0.3333	0.5
PP/PDMB	742	745	0.508	0.3333	0.1667	0.5
P2B/PEP	902	901	0.402	0.3	0.3	0.75
P2B/PPE	902	901	0.399	0.3	0.3	0.75
P2B/PIB	1214	1213	0.290	0.25	0	0
PE/PEE	1214	1213	0.228	0.25	0.25	0.1667
P2B/PEE	1214	1213	0.222	0.25	0.25	0.6667
PE/PEP	1972	1971	0.173	0.2	0.2	0.25
PE/PPE	1972	1971	0.169	0.2	0.2	0.25
P2B/PDMB	2782	2785	0.136	0.1667	0	0
PP/P2B	2782	2782	0.118	0.1667	0.1667	0.5
PPE/PP	4341	4342	0.0778	0.1333	0.1333	0.25
PEP/PP	4341	4342	0.0713	0.1333	0.1333	0.25
PP/PEE	10525	10525	0.0303	0.0833	0.0833	0.1667
PIB/PDMB	10525	10525	0.0258	0.0833	0	0
PEP/PEE	30521	30521	0.0134	0.05	0.05	0.0833
PPE/PEE	30521	30521	0.0094	0.05	0.05	0.0833
PEP/PPE	480021	480021	0.0007	0	0	0

[a] The blend branching parameter r is evaluated in the long chain limit $r \equiv r(M_1, M_2 \to \infty)$, where M_α is the site occupancy index for polymer species α, $M = (M_1 + M_2)/2$, and T_c designates the critical temperature for the blend phase separation. Values of the rule of thumb parameters p and q are also present for comparison.

we may convert eq 3.1 into an equivalent form,

$$r = \left| \frac{M_1 + M_1^{(e)} + M_1^{(tetr)}}{M_1} - \frac{M_2 + M_2^{(e)} + M_2^{(tetr)}}{M_2} \right| = \left| p_1 - p_2 + \frac{M_1^{(tetr)}}{M_1} - \frac{M_2^{(tetr)}}{M_2} \right| \quad (3.3)$$

Equation 3.3 immediately explains why the rule of thumb ratio $p = |p_1 - p_2|$ fails to correlate with the equal energy LCT miscibilities for some polyolefin systems, such as those containing PIB or PDMB. The presence of tetrafunctional carbon atoms introduces a difference between the parameters r and p. The quantity p does not properly characterize the architectural influence of tetrafunctional carbon atoms on the miscibilities of polyolefins. Similar considerations also apply to the ratio $q_i \equiv M_i^{(e)}/M_i^{(int)}$ of end to interior groups and to the difference $q = |q_1 - q_2|$. The relation between the parameter r and the fractions q_1 and q_2 can be used to express eq 3.3 as

$$r = \left| \frac{1 + 2q_1 + M_1^{(tetr)}/M_1^{(int)}}{1 + q_1} - \frac{1 + 2q_2 + M_2^{(tetr)}/M_2^{(int)}}{1 + q_2} \right| \quad (3.4)$$

again suggesting the inadequacy of employing the old rule of thumb for describing the miscibility patterns of polyolefins with nonzero $M_i^{(tetr)}$. Table 1 summarizes the parameters r_i, p_i, and q_i for the eight polyolefin species studied (see Figure 1), while Table 2 contains the resulting values of $r = |r_1 - r_2|$, $p = |p_1 - p_2|$, and $q = |q_1 - q_2|$ for the 28 possible binary polyolefin blends.

The trend of a diminishing r parameter with improved miscibility is also confirmed by the analysis of the phase

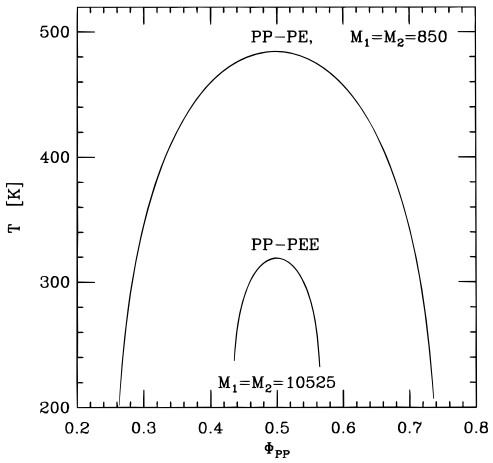

Figure 4. Comparison of LCT spinodal curves for PP/PE and PP/PEE blends at $P = 1$ atm as calculated by employing the single interaction energy model with $\epsilon = 207.75$ K.

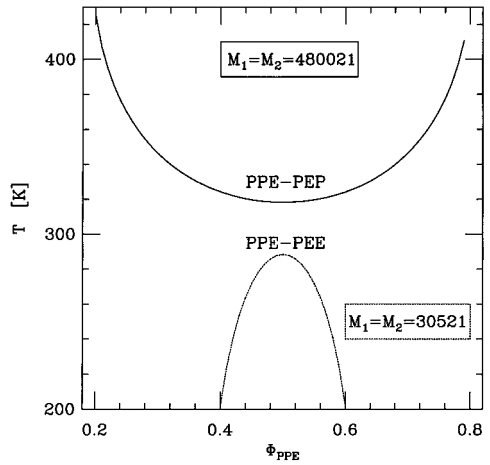

Figure 5. LCT spinodal curves for PPE/PEP and PPE/PEE blends at $P = 1$ atm as calculated by using the single interaction energy model with $\epsilon = 207.75$ K.

diagrams in Figures 2 and 3. The PP/P2B blend is the most miscible example in Figure 2 and yields $r = |^4/_3 - {}^3/_2| = 0.1667$, which is smaller than $r = |^4/_3 - {}^5/_3| = 0.3333$ for the less miscible PP/PDBM mixture. This blend, in turn, is more compatible than the PP/PIB system, which is characterized by the highest r value $r = |^4/_3 - {}^7/_4| = 0.4167$. An analogous scaling of miscibility with r emerges as well from Figure 3. The values of $r_{P2B/PIB} = 0.25$, $r_{P2B/PDMB} = 0.1667$, and $r_{PIB/PDMB} = 0.0833$ correlate well with the better miscibility of PIB/PDMB than P2B/PDMB or P2B/PIB and of P2B/PDMB than P2B/PIB.

A few additional examples illustrate the usefulness of the parameter r in estimating the miscibilities of other polyolefin blends. While the PP/PE system is rather immiscible, the PP/PEE blend is found[24] to be fairly compatible. The same trend emerges from the single interaction energy model LCT computations displayed in Figure 4. Both spinodal curves of Figure 4 exhibit upper critical solution temperatures but display a huge disparity in their miscibilities. This disparity is also consistent with the different values of the r parameter ($r_{PP/PE} = |^4/_3 - 1| = 0.3333$ versus $r_{PP/PEE} = |^4/_3 - {}^5/_4| = 0.0833$) for the two blends. A decrease in r inevitably leads to improved blend miscibility.

The limiting case of $r = 0$ is presented in Figure 5 for the PPE/PEP system. The LCST phase diagram for the PPE/PEP blend contrasts sharply with the UCST diagram for the PPE/PEE system. Note that the molecular weights for the PPE/PEP example in Figure 5 are extremely high (both M_i are on the order of half a million, which translates into polymerization indices of about 100 000). Thus, the equal energy model LCT computations predict this system to be completely miscible because of the vanishing parameter r. The comparison of the LCT phase diagrams for the PPE/PEE blend (in Figure 5) with those for the PP/PEE blend (in Figure 4) indicates the greater miscibility of PPE/PEE over PP/PEE, a trend which can be easily inferred from the values of the r parameter ($r_{PPE/PEE} = |^6/_5 - {}^5/_4| = 0.05$ versus $r_{PP/PEE} = |^4/_3 - {}^5/_4| = 0.0833$). Note that the actual PPE/PEP, PPE/PEE, etc., blends must have some degree of energetic asymmetry which, as shown in subsection C, can produce a diminished miscibility over that inferred from the single interaction energy model.

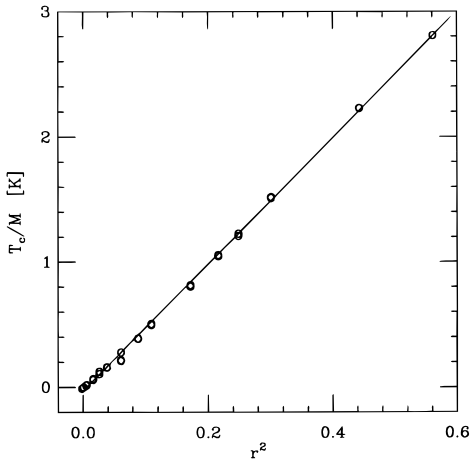

Figure 6. Correlation between the reduced critical temperature T_c/M (normalized by the number of carbons $M = M_1 = M_2$ in each chain) and the blend structural parameter r defined by eq 3.1. The calculations of T_c are performed for the single interaction energy model with $\epsilon = 207.75$ K.

As mentioned earlier, the computations of phase diagrams for all 28 binary polyolefin blends, the monomer structures of which are given in Figure 1, have been performed for different molecular weights $M = M_1 = M_2$. It is obvious that variations in M must strongly influence phase behavior. Thus, a quantitative analysis of miscibilities of these systems requires considering the ratio T_c/M rather than comparing the critical temperatures (T_c). This ratio is presented in Table 2 and in Figure 6 as a function of the blend structural parameter r that is defined in eq 3.1. The circles in Figure 6 denote the LCT computations for the single energy model, while the solid line is a least squares fit. Figure 6 demonstrates that the dependence of T_c/M on r^2 has a linear form $T_c/M = ar^2 + c$ with $c = -0.031$, and $a = 5.06$ (for $\epsilon = 0.5k_BT_0$). (A quadratic form $T_c/M = ar^2 + br + c$ yields only a marginally better fit.) The coefficients a and c vary a little when the single interaction energy departs from $\epsilon = 0.5k_BT_o$ ($T_o = 415.15$ K). For instance, $a = 5.57$ and $c = -0.034$, if $\epsilon = 0.55k_BT_o$ or $a = 4.56$, and $c = -0.028$, if a lower value of the interaction energy $\epsilon = 0.45k_BT_o$ is assumed. The normalized critical temperature T_c/M also correlates quite well with r^2 for these choices of ϵ. Notice that Figure 6 presents several examples where different blends yield the same r^2 but slightly different T_c/M. The appearance of a slight spread in T_c/M at a given r^2 arises because the LCT free energy for a binary blend also depends on other geometrical characteristics of the two polyolefin species

than the coefficients $N_2^{(1)}$ and $N_2^{(2)}$ defining[20] r. However, the dependence on r^2 is predominant. The spread in T_c/M for fixed r^2 varies with the ranges of M, but this spread effectively introduces "error bars" to the points on the curve in Figure 6. The T_c/M, r, p, and q are summarized in descending order of T_c/M for all 28 binary polyolefin blends in Table 2. The correlation with r is almost perfect. On the other hand, Table 2 explicitly demonstrates that the blend miscibilities do not correlate with the parameters p and q. In contrast to the parameter r, both these quantities exhibit no regular pattern when T_c/M decreases.

C. Energetic Asymmetries. Miscibility data for blends of PE, PEP, and PEE by Bates *et al.*[18] have been used to suggest that miscibility improves in the order PE/PEE, PEP/PEE, PE/PEP. On the other hand, the corresponding r values are 0.25, 0.05, 0.2, respectively. However, as we now describe, energetic asymmetries can be responsible for these departures because of the considerable difference between, for instance, Lennard−Jones CH_3-CH_3 and CH_2-CH_2 interaction parameters (e.g., 90 and 70 K, respectively[26]). For example, our previous work already notes that those cases found by Graessley, Lohse, and co-workers[2] to exhibit irregular mixing are the ones for which the reduced temperature T^* and/or reduced pressure P^* differ most between the two components. Disparities in T^* and P^* reflect energetic asymmetries, as explained previously in this series. Apart from considerations of energetic asymmetries, the conclusions of Bates *et al.*[18] concerning relative miscibilities, however, do not emerge from direct measurements of the critical temperatures for these three blends but from an analysis based on many debatable assumptions. These assumptions include neglecting the entropic portion of χ, equating χ for blends and diblocks, inferring relations between the order−disorder transition temperatures of the corresponding diblock copolymer systems and the critical temperatures of binary blends, ignoring the randomness introduced by the microstructure that is present in diene syntheses, etc.

As mentioned above, the various CH_n ($n = 0-3$) groups are well-known[26] to be inequivalent energetically. The systematic treatment of interaction asymmetries for a particular polyolefin binary blend requires the laborious determination of at least three (monomer-averaged) interaction energies (ϵ_{11}, ϵ_{22}, and ϵ_{12}), with the ϵ_{ii} obtained by fitting pure component thermodynamic data and the ϵ_{ij} taken from fits to blend data.[12] We focus here upon generic trends by studying the variations in phase diagrams produced by altering these interaction energies for given monomer structures.

Introducing a small asymmetry into the self-interaction energies ϵ_{11} and ϵ_{22}, while leaving the heterocontact interaction energy $\epsilon_{12} = (\epsilon_{11}\epsilon_{22})^{1/2}$ fixed as the Berthelot geometrical mean combining rule[32] for ϵ_{11} and ϵ_{22}, renders the binary UCST polyolefin blends less miscible than in the simple model with all three $\epsilon_{\alpha\beta}$ identical. This trend is illustrated in Figure 7, which depicts the variation of the critical temperature T_c as a function of the ratio $\lambda \equiv (\epsilon_{22}/\epsilon_{11})^{1/2}$ for a series of polyolefin blends with PE as a common component. The critical temperature is a minimum for $\lambda = 1.001-1.002$ in all four systems of Figure 7. Using typical values of ϵ_{ii} in the range 200−300 K implies that this minimum appears [for $\epsilon_{12} = (\epsilon_{11}\epsilon_{22})^{1/2}$] when the three interaction energies deviate by only 0.4−1.2 K, i.e., when they are basically identical. Figure 7 also indicates that the more miscible

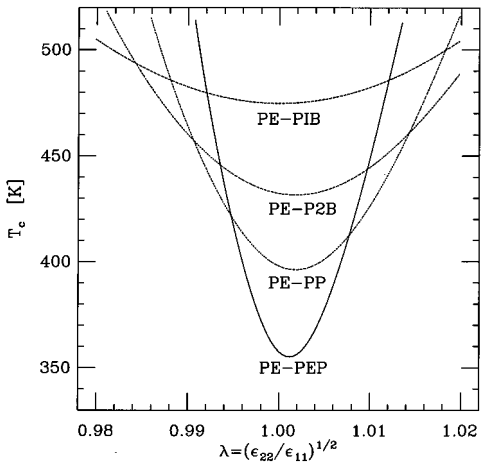

Figure 7. LCT predictions of the critical temperature as a function of the ratio $\lambda = (\epsilon_{22}/\epsilon_{11})^{1/2}$ of the microscopic self-interaction energies ϵ_{11} and ϵ_{22} for a series of polyolefin blends (at $P = 1$ atm) with PE as a common component. The self-interaction energy ϵ_{11} is chosen as $\epsilon_{11} = 207.75$ K, while the heterocontact interaction energy $\epsilon_{12} = (\epsilon_{11}\epsilon_{22})^{1/2}$ is the Berthelot combining rule geometrical mean of ϵ_{11} and ϵ_{22}. The curves are generated for different sets of site occupancy indices $M_1 = M_2 = 169$, 354, 754, and 2002 (top to bottom, respectively).

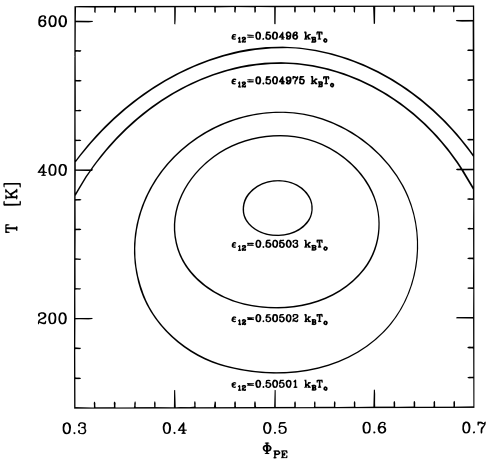

Figure 8. LCT spinodal curves for a PE/PEP blend (at $P = 1$ atm) with $\epsilon_{11} = 0.51k_BT_o$, $\epsilon_{22} = 0.5k_BT_o$ ($T_o = 415.15$ K), and ϵ_{12} as indicated in the figure. Chains of both blend components are assumed to have the same numbers ($M_1 = M_2 = 2002$) of carbon atoms.

systems display a higher sensitivity of the critical temperature T_c to the difference $\epsilon_{11} - \epsilon_{22}$ between the self-interaction energies ϵ_{11} and ϵ_{22}. Notice also that the molecular weights are much higher for the more miscible blends (see below), so the miscibility disparities in Figure 7 are much more marked than is apparent at first glance. As noted in the Introduction, a portion of the strong sensitivity to variations in interaction energies is already present in simple FH theory due to the large changes they induce in the exchange energy ϵ_{ex} of eq 1.1.

Once ϵ_{11} and ϵ_{11} are fixed, the stability limit is strongly affected by extremely small variations of the heterocontact interaction energy ϵ_{12} by the order of one part per thousand. If ϵ_{12} is less (top curve in Figure 8) than or equal (second from top curve in Figure 8) to the Berthelot combining rule[32] value $(\epsilon_{11}\epsilon_{22})^{1/2}$, the phase diagram generally only displays a maximum, i.e., an upper critical solution temperature. Interesting closed loop phase diagrams, such as those shown in Figure 8, emerge, however, as soon as ϵ_{12} becomes slightly larger

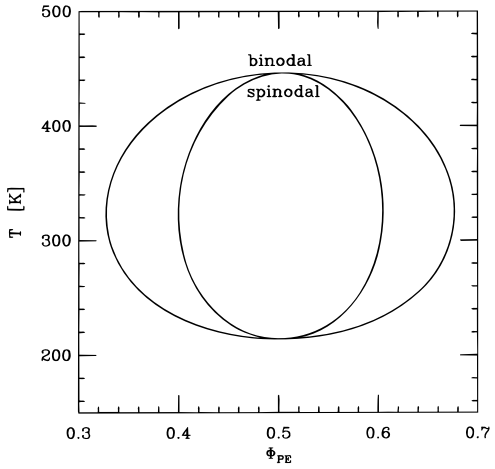

Figure 9. Comparison of the LCT binodal (coexistence curve) and the LCT spinodal for a PE/PEP blend (at $P = 1$ atm) with $\epsilon_{11} = 0.51k_BT_o$, $\epsilon_{22} = 0.5k_BT_o$, and $\epsilon_{12} = 0.50502k_BT_o$ (T_o = 415.15 K). Chains of both blend components are assumed to have the same numbers ($M_1 = M_2 = 2002$) of carbon atoms.

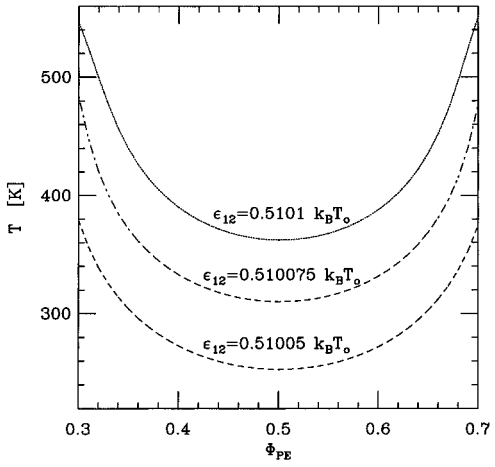

Figure 10. LCT spinodal curves for a PE/PEP blend (at $P =$ 1 atm) with $\epsilon_{11} = 0.52k_BT_o$, $\epsilon_{22} = 0.5k_BT_o$, and ϵ_{12} as indicated in the figure. The molecular weights of PE and PEP are the same as in Figures 8 and 9.

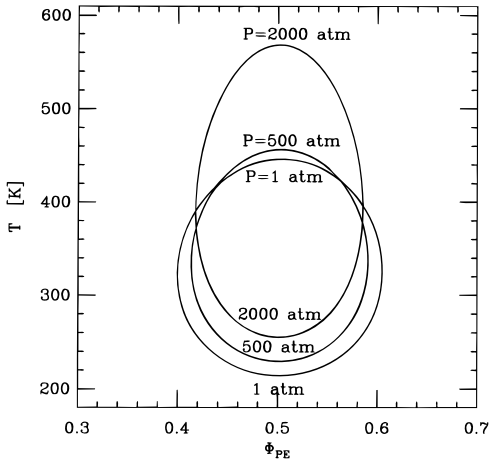

Figure 11. LCT predictions for the pressure variations of a closed loop phase diagram for a PE/PEP blend with microscopic interaction energies and molecular weights as in Figure 9.

than the geometrical mean $(\epsilon_{11}\epsilon_{22})^{1/2}$ and the exchange energy ϵ_{ex} becomes negative. The largest of the closed loop phase diagrams in Figure 8 corresponds to ϵ_{12} only 0.014 K smaller than the Berthelot geometrical mean, a miniscule value that emphasizes the strong sensitivity of blend miscibilities to subtle differences in the microscopic interactions. A further increase of ϵ_{12} leads to the smaller closed loop diagrams in Figure 8 and eventually to complete blend miscibility. The predicted emergence of the closed loop phase diagrams for model polyolefin blends generally requires a small degree of asymmetry in all three interaction energies, an asymmetry that is physically quite reasonable based on the large range of different $(CH_n)-(CH_n)$ Lennard−Jones parameters used in off-lattice united atoms models. Similar trends are found for all the binary polyolefin blends studied. The closed loop phase behavior of polyolefin blends has also been observed experimentally.[1,33] The small deviations from the Berthelot rule ϵ_{12} required to produce closed loop or LCST phase diagrams accord with the analysis of Graessley, Lohse, and co-workers[1,2] of similar small magnitudes for the correction terms to the solubility parameter model in treating the examples of "irregular" mixing. For example, each monomer of PIB has a pair of methyl side groups which have stronger interactions than the CH_2 and C backbone groups, producing a higher reduced temperature T^* for PIB melts than for the other polyolefins studied by Graessley and co-workers. Thus, in conformity with the LCT computations, blends of PIB with other polyolefins display the largest energetic asymmetries and are consequently most susceptible to exhibiting LCST and closed loop phase diagrams.[2,33]

Figure 9 compares the spinodal and coexistence curves for one of the examples from Figure 8. Both curves coincide with each other at each of the two critical points. Depending on the molecular weights and interaction energies, only the lower or higher critical temperature may appear in an experimentally accessible region between the glass transition temperature and a decomposition temperature. Figure 10 presents an example with apparent LCST phase behavior because the UCST branch of the phase diagram lies at elevated temperatures that probably exceed the decomposition temperature and is, therefore, not depicted in Figure 10. While Figures 9 and 10 are presented for a PE/PEP blend, similar behaviors again appear when energetic asymmetries are introduced into the LCT calculations for other binary systems formed from polyolefins in Figure 1.

Our previous computations with the single interaction energy model indicate that an increase of pressure disfavors[20] polyolefin blend miscibility. A similar trend is maintained for systems exhibiting closed loop phase diagrams, especially in the range of higher pressures. Both the lower and upper critical solution temperatures grow with pressure, but the latter increases more rapidly (see Figure 11) and dominates the overall change of miscibility with pressure. The shape of the phase diagram changes as well, shrinking in one direction, but expanding in another. The pressure variation of the lower critical solution temperature is also consistent with our previous computations[12] for a typical LCST blend, PS/PVME.

When energetic asymmetries are present in a blend, the equal interaction energy correlation in Figure 6 must be modified for the resultant shift in T_c. For example, consider the simple case of Figure 7, where ϵ_{11} and ϵ_{22} vary from each other by less than a few percent ($0.98 < \lambda \equiv (\epsilon_{22}/\epsilon_{11})^{1/2} < 1.02$) but the heterocontact interaction energy $\epsilon_{12} = (\epsilon_{11}\epsilon_{22})^{1/2}$ is taken as the geometrical mean. The second derivative $d^2T_c/d\lambda^2$, which describes the curvature of the functions $T_c(\lambda)$ in Figure 7, is found to decrease exponentially with r as A

$\exp[-br + cr^2]$ ($b > c$). Hence, this latter dependence may be used as a rough guide for the shift of T_c due to energetic asymmetries. However, as noted above, deviations from the geometric mean combining rule for the heterocontact energies may qualitatively alter the nature of the phase diagrams, so some measure of experimental data is useful to fit the interaction energies (and thereby also subsume some deficiencies of the lattice model into the fit).

IV. Computations of Interfacial Properties

The importance of monomer structural asymmetries and blend compressibility in describing polyolefin blend miscibility patterns implies the necessity of treating their interfacial properties with a theory that accounts for blend compressibility and the pressure dependence. The interfacial profiles, widths, and tensions of phase-separated polyolefin blends have been computed by using a compressible blend theory[25] and by assuming, for convenience, that the system conforms to the weak segregation limit ($R_G^{(i)} \ll \omega$). The latter assumption is, however, irrelevant for probing how monomer structures (and various miscibility patterns induced by the structural asymmetries of polyolefin blends) affect the interfacial properties of phase-separated binary blends. The theoretical distinction between the weak and strong segregation limits lies only in the presence of a different constant k in eq 2.10 and, therefore, considering either of these two cases produces similar qualitative trends.

The computations are illustrated for a series of four polyolefin blends having PE as a common component (component 1) and PEP, PP, P2B, and PIB as the second blend species. The Kuhn lengths

$$l_\alpha = R_G^{(\alpha)}/[(1/6)N_\alpha]^{1/2} \qquad (4.1)$$

represent necessary input parameters to the calculations of interfacial characteristics. Since the exact computation of $R_G^{(i)}$ for the structured monomer chains is, unfortunately, extremely tedious, the $R_G^{(i)}$ are estimated by using an approximate non-self-reversing random walk model and assuming that only bond vectors attached to a common lattice site are correlated. This approximation is correct to leading order in z^{-1}, and the procedure produces the same expression for R_G for all the polyolefins considered

$$R_G{}^2 = (1/6)a_{cell}{}^2 M_{bb}[1 + 2/z + ...]^{1/2} \qquad (4.2)$$

where $a_{cell} = (v_{cell})^{1/3}$ is the lattice constant, z is the lattice coordination number, and M_{bb} denotes the number of carbon atoms in the chain backbone. Equations 4.2 and 4.1 lead to $l_{PE} = l_{PP} = l_{P2B} = l_{PIB} = 4.1604$ Å, and $l_{PEP} = 5.8837$ Å for our choice of $a_{cell} = 2.5477$ Å and $z = 6$. These Kuhn lengths do not reflect the experimental values because of the simplications posed by the lattice model and the obvious limitations of the truncation in eq 4.2. Since a more accurate treatment of $R_G{}^2$ is quite complicated, the present Kuhn lengths adequately serve to illustrate the general trends.

Because the theory of interfacial properties requires knowledge of the compositions of the coexisting phases, Figure 12 presents a series of binodal curves that again indicate the computed miscibilities of PE/PEP, PE/PP, PE/P2B, and PE/PIB as diminishing in this order. Figure 12, however, de-emphasizes the actual compatibility differences of these four mixtures since their molecular weights are not chosen as identical in order to prevent the critical temperatures for the less miscible systems from exceeding the decomposition temperatures. For instance, the molecular weights $M_1 = M_2$ for PE/PIB (the least miscible blend in Figure 12) are an order of magnitude lower than $M_1 = M_2$ for the most miscible PE/PEP blend. The coexistence curves of Figure 12 describe the compositions $\Phi_1^{(I)}$, $\Phi_2^{(I)} = 1 - \Phi_1^{(I)}$, $\Phi_1^{(II)}$, and $\Phi_2^{(II)} = 1 - \Phi_1^{(II)}$ of the coexisting phases I and II at a given temperature $T < T_c$ and the pressure $P = 1$ atm. The equation of state provides the free volume fractions $\phi_v^{(I)}$ and $\phi_v^{(II)}$ in both homogeneous phases.

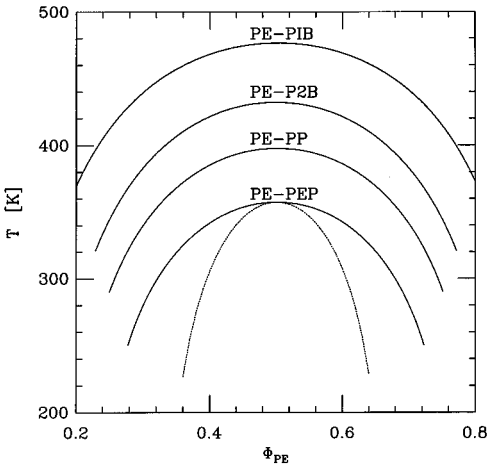

Figure 12. LCT coexistence curves (binodals) at $P = 1$ atm for a series of polyolefin blends with PE as the common component 1. All curves are generated by using the single interaction energy model with the same microscopic interaction energy $\epsilon = 207.75$ K, but for different sets of site occupancy indices, $M_1 = M_2 = 169$, 354, 754, and 2002 (top to bottom, respectively). The same sets of occupancy indices and the same interaction energy ϵ apply to Figures 13–16. For comparison, the bottom curve illustrates the spinodal for PE/PEP.

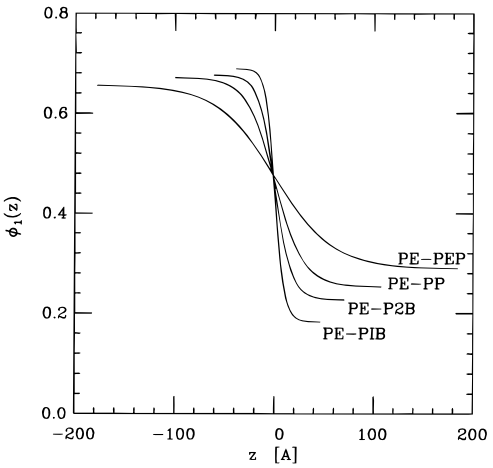

Figure 13. Interfacial profiles $\phi_1(z)$ for a series of polyolefin blends with PE as the common component 1 at $P = 1$ atm and the same relative temperature $\theta = T/T_c = 0.8$. Since the critical temperatures (T_c) vary for these blends, the constancy of θ implies different temperatures T for each blend.

The interfacial profiles $\phi_i(z)$ ($i = 1, 2$) converge to the limiting bulk values $\phi_i^{(I)} = \Phi_i^{(I)}/(1 - \phi_v^{(II)})$ for sufficiently large $|z|$. Figure 13 illustrates the computed interfacial profiles $\phi_1(z)$ for four polyolefin systems at a constant reduced temperature of $\theta \equiv T/T_c = 0.8$ and at $P = 1$ atm. The broadest and steepest profiles correspond, respectively, to the most and least miscible blends, as expected. An analogous behavior is displayed by the profile $\phi_2(z)$ of the second component.

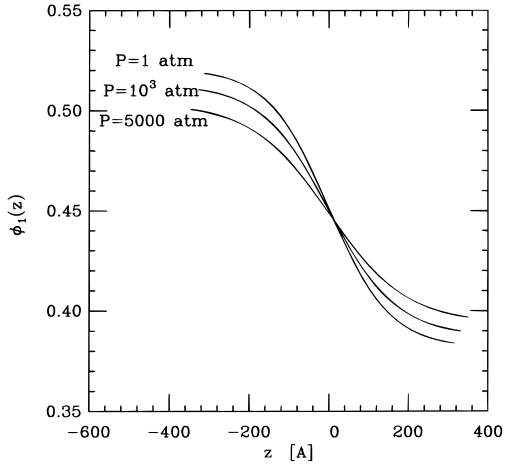

Figure 14. A typical pressure variation of the interfacial profile $\phi_1(z)$ for a PE/PEP blend at $T = 348.5$ K.

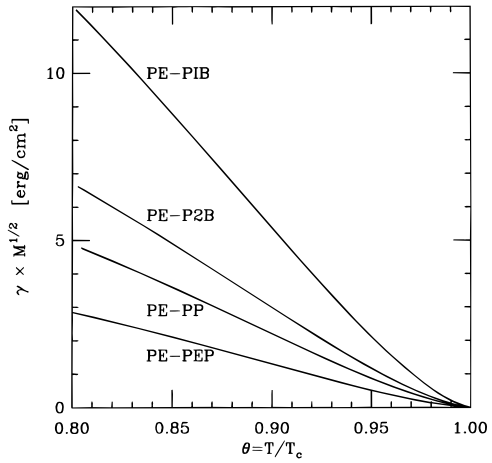

Figure 15. Temperature variation of the interfacial tension (γ) (multiplied by the square root of the number of carbon atoms $M \equiv M_1 = M_2$) for a series of polyolefins blended (at $P = 1$ atm) with PE as a common component. The multiplication of γ by $M^{1/2}$ represents an attempt to eliminate the dependence of γ on the molecular weights, which are assumed to be different (see Figure 12) for these four blends.

Figure 14 shows the pressure dependence of the PE profile. An increase in pressure makes both profiles $\phi_1(z)$ and $\phi_2(z)$ broader, but this behavior is basically driven by the changing coexisting phase compositions as the pressure is varied.

The interfacial tensions γ and widths ω also correlate with the blend miscibility. Figures 15 and 16 depict, respectively, the interfacial tensions ($\gamma' = \gamma M^{1/2}$) and the interfacial widths ($\omega' \equiv \omega/\bar{R}_G$) as a function of the relative temperature ($\theta = T/T_c$). The multiplication of the interfacial tensions (γ) by the square root of the average molecular weight ($M = (M_1M_2)^{1/2}$) and the division of the interfacial widths (ω) by the averaged radius of gyration ($\bar{R}_G = [R_G^{(1)} R_G^{(2)}]^{1/2}$) are employed to compensate for the influences of differences in the molecular weights chosen for the four systems. (This procedure does not fully remove variations due to the finite polymerization indices, as estimated from the interpolation formulas of Tang and Freed[34] for the incompressible limit.) As expected, γ' diminishes at a given reduced temperature $\theta < 1$ as the miscibility improves, while ω' increases. The normalization in Figure 16 is also useful for recognizing the cases for which the weak segregation limit applies, i.e., for which $\omega \gg [R_G^{(1)} R_G^2]^{1/2}$.

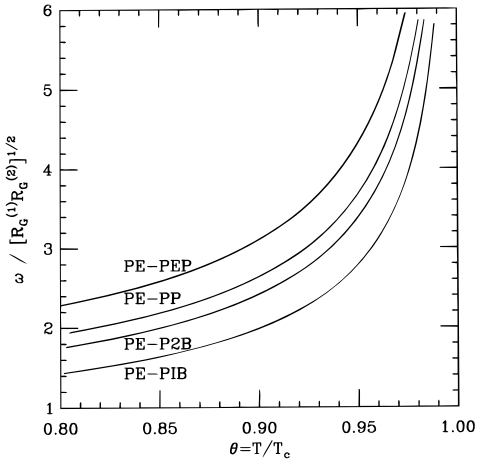

Figure 16. Temperature variation of the interfacial width (ω) (divided by the averaged radius of gyration $\bar{R}_G = [R_G^{(1)} R_G^{(2)}]^{1/2}$) for a series of polyolefin blends (at $P = 1$ atm) with PE as the common component 1.

V. Discussion

The apparent chemical similarity of polyolefins poses important questions concerning the relation between monomer molecular structures and the miscibilities of polyolefin blends when it is realized that polyolefin blends exhibit widely varying miscibilities and different types of phase diagrams with lower (LCST) and upper (UCST) critical temperatures, or even with both. (The LCST phase diagrams have a higher UCST critical temperature outside of the physically realistic range.) The syntheses of most of the polyolefins studied are based on the hydrogenation of dienes, so these polyolefins are random copolymers rather than pure homopolymers. Even high-density polyethylene contains small amounts of branches, randomly distributed along the chain, and, consequently, some degree of randomness. The description of random copolymer blends requires the use of a much more sophisticated theory. Such a theory is currently under development, and preliminary studies[35] indicate the molecular origins of monomer sequence dependent terms in the free energy, terms which are numerous and which can strongly influence the calculated thermodynamic properties. A similar conclusion follows from experiments of Lohse and coworkers,[36] who have studied the miscibility of atactic propylene with several ethylene−propylene copolymers, varying in monomer sequence from strictly alternating copolymers to diblocks, with a range of statistical copolymers in between. The diblock is found to be the least miscible, and the alternating copolymer, the most.

Our investigation of the factors governing polyolefin blends has begun in our previous work,[20] where the lattice cluster theory (LCT) is used with united atom models of the monomers (see Figure 1). The computations in that paper assume the polyolefins to be nonrandom pure homopolymers and employ a single interaction energy model for the interaction energies in order to isolate the role that monomer molecular structure plays in controlling polyolefin miscibilities. The present paper continues analyzing the influence of monomer structural asymmetries on polyolefin blend phase diagrams by studying a wider range of monomer structures with longer branches and by further testing an older rule of thumb relating polyolefin miscibilities to disparities in a parameter p_i that equals the ratio of the number of terminal carbon atoms to the total number of carbons in a chain of species i. The failure of this

rule of thumb in correlating the LCT computations has led to the development of better criteria for predicting the LCT polyolefin miscibilities. The analysis then proceeds to a consideration of the combined influence of structural and energetic asymmetries in view of the differing interactions required for describing the polyolefin united atom groups in continuum model simulations.[26]

The equal energy model assumes that different CH_n united atom groups interact with the same microscopic van der Waals energy (ϵ). A wide range of LCT binary blend phase diagrams calculated with this model yield constant pressure critical temperature $(T_c(P)/M)$ that exhibit a linear dependence on the blend structural parameter (r^2) of eq 3.1,

$$\frac{T_c(P)}{M} = ar^2 + c \quad (a > 0, c < 0) \tag{5.1}$$

where the number (M) of carbons in a polyolefin chain is taken as identical for the two blend species ($M_1 = M_2 = M$). The ratio of the critical temperature (T_c) and the number (M) of carbons (in a single chain) is an increasing function of r^2, and both coefficients a and c are found to vary only slightly with ϵ for a given pressure. The limiting case of $r = 0$ corresponds to a completely miscible system. The LCT computations have been performed for ϵ between 185 and 230 K to ensure that the blend has liquid-like densities and that the computed critical temperatures lie in the range 240−540 K for all the binary blends and molecular weights considered in the computations summarized in Figure 6.

The quantity r^2 represents a measure of the disparity between the monomer structures of the two blend components. Another measure of this same disparity is the entropic portion of the effective interaction parameter χ_{eff} which emerges in the high pressure, high molecular weight limit as also being proportional to r^2. The parameter r is shown here to be evaluated easily for an arbitrary pair of polyolefin species simply by counting the fractions of tri- and tetrafunctional carbon atoms in both polyolefin species chains (see eq 3.1). These fractions appear as $r_i = (M_i^{(tri)} + 3M_i^{(tetr)})/M_i$ in eq 3.1 defining $r = |r_1 - r_2|$ and are trivially determined directly from the individual monomer structures (such as those depicted in Figure 1). (Contributions to r from chain ends are negligible as may be seen from Table 1 of the first paper of this series, which compares the values of r for a series of polyolefin blends with finite and infinite molecular weights.) The great simplicity of evaluating the parameter r makes the correlation (5.1) trivial to apply.

The new correlation in eq 5.1, along with the definition of r in eq 3.1, immediately explains the failure of the older rule of thumb for predicting the miscibilities of some LCT equal energy model polyolefin blends. The ratio p_i of end to total (or interior) CH_n groups in a polyolefin chain departs from r_i when the chain contains tetrafunctional carbons. Figures 2 and 3 exhibit examples of polyolefin blends for which the miscibilities strongly deviate from patterns suggested by the older rule of thumb because of the presence of interior tetrafunctional carbons.

Among the 28 binary polyolefin blends analyzed in Figure 6, there are several pairs of blends and a few combinations of three different blends that yield identical r^2 but slightly different reduced critical temperature T_c/M. The small spreads of T_c/M for fixed r^2 in Figure 6 stem from the fact that the LCT free energy (and its second derivative $\partial\mu_1/\partial\Phi_1$) depends on the monomer structures of the two blend components through a whole set of geometrical coefficients N_2, N_3, N_{11}, N_{12}, etc. (defined in ref 3), while the definition of the structural parameter r^2 involves only the leading coefficient N_2, which fortunately appears to dominate the computed blend miscibilities. The correlation (5.1), however, must be treated as a first approximation for describing real polyolefin systems which exhibit both structural and energetic asymmetries.

The Bates−Fredrickson model[18] for polyolefin miscibilities focuses on the parameters $R_{G,i}^2/V_i$, where $R_{G,i}$ and V_i are the radius of gyration and molecular volume, respectively, of a chain of component i. The polyolefin blend miscibility is determined in terms of disparities of these parameters between the two blend components. Schweizer and Singh[19] test the conclusions of the Bates−Fredrickson model by applying PRISM computations and analytical approximations to semiflexible hard sphere chain systems. While the structured monomer models used in the LCT computations impart some degree of stiffness to the polymer chains, precise (and very difficult) computations of R_G for these structured monomer models lie beyong the scope of the present study. Thus, the present paper investigates the monomer structural influences on polyolefin miscibilities that complement those treated by PRISM methods. Clearly, it is desirable to study polyolefin miscibilities using more realistic models that combine chain stiffness differences, monomer structure, and interaction asymmetries, as well as both entropic and enthalpic consequences of nonrandom mixing and compressibility. Such work is in progress[22] with the incorporation of bending energies into the LCT.

A typical single interaction energy model LCT phase diagram for a binary polyolefin blend exhibits an UCST in accord with the majority of experimental observations[1,2] and predictions[37] of other theories. The correlation of eq 5.1 becomes altered when energetic asymmetries are introduced into the LCT computations, except perhaps for blends where the self-interaction energies ϵ_{11} and ϵ_{22} depart from each other by only a few percent and where the heterocontact interaction energy satisifies the Berthelot combining rule $\epsilon_{12} = (\epsilon_{11}\epsilon_{22})^{1/2}$. No regular pattern is displayed by the LCT miscibilities of blends when ϵ_{12} differs from the geometrical mean $(\epsilon_{11}\epsilon_{22})^{1/2}$ and when ϵ_{11} and ϵ_{22} vary by more than about 5% from equality. For instance, Figures 8 and 10 demonstrate that three different classes of phase behavior (UCST, LCST, and closed loop phase diagrams) can be generated from the LCT by introducing a slight variation of the three $\epsilon_{\alpha\beta}$, a variation which is not necessarily unrealistic in view of the fact that typical off lattice $(CH_3)-(CH_3)$ and $(CH_2)-(CH_2)$ Lennard Jones energy parameters are 90 and 70 K, respectively.[26] Both LCT computed spinodal and binodal curves are found to be extremely sensitive to miniscule changes of ϵ_{12} when ϵ_{11} and ϵ_{22} are fixed and when the exchange energy $\epsilon_{ex} \equiv \epsilon_{11} + \epsilon_{22} - 2\epsilon_{12}$ changes its sign. This expected sensitivity is, of course, also present in FH theory. The LCT phase behavior is likewise profoundly affected by the overall difference (ϵ_{ex}), which is generally orders of magnitude smaller than the individual $\epsilon_{\alpha\beta}$. As in FH theory, the LCT free energy expression contains the leading random mixing term $(1/2)\epsilon_{ex}z\phi_1\phi_2/(k_BT)$ along with many nonrandom-mixing terms. The nonrandom-mixing contributions in the LCT are responsible

for the appearance of nontrivial phase diagrams, even for the equal energy model which yields $\epsilon_{ex} = 0$ and which would therefore predict complete miscibility within FH theory.

Despite the major conceptual advances described in this and the preceding papers, the LCT does have deficiencies (as do all model-based theories!), most of which would appear to arise from the simplifications induced by the underlying lattice model. For example, Hall and co-workers[38] have devised descriptions for the equation of state for homopolymer melts, based on continuum space hard sphere chain models. These new descriptions should be far more accurate than those derived from the lattice model with its translational entropy term $\phi_v \ln \phi_v$, where ϕ_v is the fraction of unoccupied lattice sites. However, fits[12] of the LCT to equation of state data for polystyrene (PS) and for poly(vinyl methyl ether) (PVME) melts exhibit no need for such an improved description of the translational entropy. Perhaps, there are cancellations of errors in the fits to experiments, but, to date, we have found no qualitative thermodynamic features, predicted by hard sphere or Lennard−Jones continuum model treatments, that are not exhibited by the current LCT, except for certain properties involving chain stiffness. (These are, however, under investigation[22] by introducing trans−gauche energy differences into the LCT.) For example, where comparisons have been made, the LCT computations provide the general qualitative trends displayed by simulations and by the continuum hard core chain PRISM theories[39] of blend thermodynamics, but the greater analytical tractability of the LCT enables the rapid computation of *constant pressure* phase diagrams, which are currently inaccessible to molecular off-lattice theories. The continuous, e.g., Edwards-type, Gaussian chain models, on the other hand, cannot describe important details of packing constraints that are known to dictate the structure of small molecule and polymer fluids. Polyolefin blends are an excellent example where these simple packing constraints can explain (even with the equal energy model) a wide variety of miscibility patterns. The continuous thread PRISM model yields an alternative analytically tractable theory for describing certain aspects of polyolefin miscibilities, but this approach, as well as more recent attempts to describe monomer structure in PRISM calculations,[40] does not provide a means for correlating molecular properties with the experimentally measured constant pressure phase diagrams.

Acknowledgment. This research is supported, in part, by NSF DMR Grant No. 95 30403. We are grateful to Jack Douglas, Boris Veytsman, and Ken Schweizer for helpful comments on the manuscript and David Lohse for providing us his unpublished results.

References and Notes

(1) Krishnamoorti, R.; Graessley, W. W.; Balsara, N. P.; Fetters, L. J.; Lohse, D. J. *Macromolecules* **1994**, *27*, 3073. Graessley, W. W.; Krishnamoorti, R.; Balsara, N. P.; Butera, R. J.; Fetters, L. J.; Lohse, D. J.; Schulz, D. N.; Sisano, J. A. *Macromolecules* **1994**, *27*, 3896. Graessley, W. W.; Krishnamoorti, R.; Reicchart, G. C.; Balsara, N. P.; Fetters, L. J.; Lohse, D. J. *Macromolecules* **1995**, *28*, 1260.

(2) Krishnamoorti, R.; Graessley, W. W.; Fetters, L. J.; Garner, R. J.; Lohse, D. J. *Macromolecules* **1995**, *28*, 1252.

(3) Dudowicz, J.; Freed, K. F. *Macromolecules* **1991**, *24*, 5076.

(4) A complementary molecular approach is given by Schweizer and Singh (*Macromolecules* **1995**, *28*, 2063), who use microscopic PRISM theory to understand certain facets of experimental data for polyolefin blends. Previous[20] and present work analyze the important monomer structural characteristic affecting polyolefin (and general) blend miscibilities, whereas Schweizer and Singh focus primarily on the influence of chain stiffness.

(5) Flory, P. J. *Principles of Polymer Chemistry*; Cornell University Press: Ithaca, NY, 1953.

(6) Sanchez, I. C.; Lacombe, R. H. *Macromolecules* **1978**, *11*, 1145.

(7) Freed, K. F.; Dudowicz, J. *Trends Polym. Sci.* **1995**, *3*, 248.

(8) Dudowicz, J.; Freed, K. F. *Macromolecules* **1990**, *23*, 1519.

(9) Schweizer, K. S. *Macromolecules* **1993**, *26*, 6033; 6050.

(10) Kumar, S. *Macromolecules* **1994**, *27*, 260.

(11) Dudowicz, J.; Freed, M. S.; Freed, K. F. *Macromolecules* **1991**, *24*, 5096.

(12) Dudowicz, J.; Freed, K. F. *Macromolecules* **1995**, *28*, 6625.

(13) Janssen, S.; Schwahn, D.; Mortensen, K.; Springer, T. *Macromolecules* **1993**, *26*, 5587.

(14) Hammouda, B.; Bauer, B. J. *Macromolecules* **1995**, *28*, 4505.

(15) Dudowicz, J.; Freed, K. F. *Macromolecules* **1991**, *24*, 5112.

(16) Dudowicz, J.; Freed, K. F. *Macromolecules* **1993**, *26*, 213.

(17) Russell, T. P.; Karis, T. E.; Gallot, Y.; Mayes, A. M. *Nature* **1994**, *368*, 729. Karis, T. E.; Russell, T. P.; Gallot, Y.; Mayes, A. M. *Macromolecules* **1995**, *28*, 1129.

(18) Bates, F. S.; Schultz, M. F.; Rosedale, J. H.; Almdal, K. *Macromolecules* **1992**, *25*, 5547. Gehlsen, M. D.; Bates, F. S. *Macromolecules* **1994**, *27*, 3611. Bates, F. S.; Fredrickson, G. H. *Macromolecules* **1994**, *27*, 1065. Fredrickson, G. H.; Liu, A. J.; Bates, F. S. *Macromolecules* **1994**, *27*, 2503. Fredrickson, G. H.; Liu, A. J. *J. Polym. Sci. Polym. Phys.* **1995**, *33*, 1203.

(19) Schweizer, K. S. *Macromolecules* **1993**, *26*, 6050. Schweizer, K. S.; Singh, C. *Macromolecules* **1995**, *28*, 2063. Singh, C.; Schweizer, K. S. *Macromolecules* **1995**, *28*, 8692. Singh, C.; Schweizer, K. S. *J. Chem. Phys.* **1995**, *103*, 5814.

(20) Freed, K. F.; Dudowicz, J. *Macromolecules* **1996**, *29*, 625.

(21) Bawendi, M. G.; Freed, K. F. *J. Phys. Chem.* **1987**, *86*, 3720.

(22) Foreman, K. W.; Freed, K. F. *J. Chem. Phys.* (submitted).

(23) Thayer, A. M. *Chem. Eng. News* **1995**, *11*, 15. Subramanian, P. S.; Chou, K. J. *Trends Polym. Sci.* **1995**, *3*, 248.

(24) Brandrup, J.; Immergut, E. H., Eds. *Polymer Handbook*; Wiley: New York, 1989.

(25) Lifschitz, M.; Freed, K. F. *J. Chem. Phys.* **1993**, *98*, 8994. Lifschitz, M.; Freed, K. F.; Tang, H. *J. Chem. Phys.* **1995**, *103*, 3767. Lifschitz, M.; Freed, K. F. *J. Chem. Phys.* **1996**, *105*, 1633.

(26) Toxvaerd, S. *J. Chem. Phys.* **1990**, *93*, 4290. Jorgensen, W. L. *J. Am. Chem. Soc.* **1981**, *103*, 335. Mondello, M.; Grest, G. S. *J. Chem. Phys.* **1995**, *103*, 7156.

(27) Hamada, F.; Shiomi, T.; Fujisawa, K.; Nakajima, A. *Macromolecules* **1980**, *13*, 729. Shiomi, T.; Fujisawa, K.; Hamada, F.; Nakajima, A. *J. Chem. Soc. Faraday Trans. 1* **1980**, *76*, 885. Fujisawa, K.; Shiomi, T.; Hamada, F.; Nakajima, A. *Polym. Bull.* **1980**, *3*, 261.

(28) Lupis, C. H. P. *Chemical Thermodynamics of Materials*; PTR Prentice Hall: Englewood Cliffs, NJ, 1983.

(29) Dudowicz, J.; Lifschitz, M.; Freed, K. F.; Douglas, J. F. *J. Chem. Phys.* **1993**, *99*, 4804.

(30) Tang, H.; Freed, K. F. *J. Chem. Phys.* **1991**, *94*, 1572.

(31) Nemirovsky, A. M.; Dudowicz, J.; Freed, K. F. *Phys. Rev. A* **1992**, *45*, 7111.

(32) Rowlinson, J. S.; Swinton, F. L. *Liquids and Liquid Mixtures*, 3rd ed.; Butterworthd: London, 1982.

(33) Lohse, D.; Graessley, W. W., private communication.

(34) Tang, H.; Freed, K. F. *J. Chem. Phys.* **1991**, *94*, 6307. See also, Lifschitz, M.; Freed, K. F.; Tang, H. *J. Chem. Phys.* **1995**, *103*, 3767.

(35) Dudowicz, J.; Freed, K. F. *Macromolecules*, in press.

(36) Lohse, D., unpublished results.

(37) PRISM computations yield UCST behavior as the most common, but more complex behavior is *possible* when chain aspect ratios are allowed to become temperature dependent in a highly system specific manner [Schweizer, K. S., private communication].

(38) Dickman, R.; Hall, C. K. *J. Chem. Phys.* **1986**, *85*, 4108. Honnell, K. G.; Hall, C. K. *J. Chem. Phys.* **1989**, *90*, 1841. Yethiraj, A.; Hall, C. K. *J. Chem. Phys.* **1991**, *95*, 8494. Zhou, Y.; Smith, S. W.; Hall, C. K. *Mol. Phys.* **1995**, *86*, 1157.

(39) Schweizer, K. S.; Curro, J. G. *Adv. Polym. Sci.* **1994**, *116*, 319. *Chem. Phys.* **1990**, *149*, 105. Yethiraj, A.; Schweizer, K. S. *J. Chem. Phys.* **1993**, *98*, 9080.

(40) Rajasekaran, J. J.; Curro, J. G.; Honeycutt, J. D. *Macromolecules* **1995**, *28*, 6843. Rajasekaran, J. J.; Curro, J. G. *J. Chem. Soc. Faraday Trans.* **1995**, *91*, 2427. Curro, J. G. *Macromolecules* **1994**, *27*, 4665.

MA961205O